

THE ORIGIN OF COLOR GRADIENTS IN EARLY-TYPE SYSTEMS AND THEIR COMPACTNESS AT HIGH-Z

LA BARBERA, F.¹, DE CARVALHO, R.R.²

INAF – Osservatorio Astronomico di Capodimonte, Napoli, Italy, and
Instituto Nacional de Pesquisas Espaciais - INPE/MCT, Sao Paulo, Brazil

Draft version October 25, 2018

ABSTRACT

In this *Letter*, we present mean optical+NIR color gradient estimates for 5080 early-type galaxies (ETGs) in the *grizYJHK* wavebands of the Sloan Digital Sky Survey (SDSS) plus UKIRT Infrared Deep Sky Survey (UKIDSS). The color gradient is estimated as the logarithmic slope of the radial color profile in ETGs. With such a large sample size, we study the variation of the mean color gradient as a function of waveband with unprecedented accuracy. We find that (i) color gradients are mainly due, on average, to a metallicity variation of about -0.4 dex per decade in galaxy radius; and (ii) a small, but significant, positive age gradient is present, on average, in ETGs, with the inner stellar population being slightly younger, by ~ 0.1 dex per radial decade, than the outer one. Also, we show that the presence of a positive mean age gradient in ETGs, as found in the present study, implies their effective radius to be smaller at high z , consistent with observations.

Subject headings: galaxies: clusters: general—galaxies: evolution—galaxies: fundamental parameters

1. INTRODUCTION

Since the early 1970's, observations have shown that the color of ETGs reddens from the outskirts to the galaxy center (Faber 1972). Understanding the origin of such color gradient can strongly constrain the scenario of galaxy formation and evolution (see La Barbera et al. 2004). Most studies to date have been plagued by the large uncertainties due to small sample sizes and short wavelength baselines where color gradients are derived. Despite these limitations they suggest that color gradients in ETGs originate from metallicity variations (Peletier et al. 1990; Tamura et al. 2000; Tamura & Ohta 2003). Small, positive age gradients are also consistent with observations (e.g. Saglia et al. 2000), though their presence has never been revealed in the family of ETGs as a whole. Positive age gradients are a robust prediction of the hierarchical paradigm of galaxy formation, as a consequence of the centrally peaked star formation of dissipative merging events.

Recent studies have shown a significant, intrinsic evolution of ETG sizes, with high redshift galaxies being more compact (by $\sim 50\%$ at $z \sim 1$) than those of analogous stellar mass at $z \sim 0$. The origin of this variation in size is still a matter of debate and may be the result of different mechanisms (see e.g. Trujillo 2009), specifically (i) the effect of minor dry mergers; or (ii) a puffing-up mechanism due to AGN feedback (Fan et al. 2008); or (iii) the increased amount of dissipation involved in gas-rich mergers forming ETGs at high-redshift (Khochfar and Silk 2006).

In this Letter, we use data from the SDSS and UKIDSS surveys to address the origin of the mean color gradient in ETGs in the nearby Universe ($z < 0.1$), connecting it to the observed compactness of their high-redshift counterparts¹. The combination of sample size, homogeneity of data, and large wavelength baseline, from optical to near-infrared (g through K bands), results in an unprece-

dent accuracy in detecting both metallicity and age variations inside galaxies. In fact, while optical (SDSS) data are very sensitive to the effects of both metallicity (through line blanketing) and age, the NIR (UKIDSS) wavebands are dominated by the old, quiescent stellar populations, allowing the effects of age and metallicity to be effectively separated (see e.g. Peletier et al. 1990).

2. THE SAMPLE

The sample of ETGs was defined from SDSS-DR6 with photometry and spectroscopy available. We selected all galaxies in the redshift range of 0.05 to 0.095, with r-band Petrosian magnitude² $M_r < -20$. The choice of the lower redshift minimizes the aperture bias (Gómez et al. 2003), while the upper redshift limit makes the sample approximately volume-complete, since the value of $M_r = -20$ roughly corresponds to the apparent magnitude limit of the SDSS spectroscopy ($r \sim 17.8$) at $z = 0.1$. Following Bernardi et al. (2003), ETGs are those galaxies with SDSS parameters $e_{class} < 0$ and $fracDev_r > 0.8$. Also, we selected only those galaxies with spectroscopic warning flags set to zero, and with available velocity dispersion, in the range of 70 to 420 km/s. These requirements yield a sample of 39,993 ETGs. We matched this sample to the fourth data release of the UKIDSS–Large Area Survey (Lawrence et al. 2007), which provides NIR photometry in the *YJHK* bands over a sky region significantly overlapping the SDSS. The matching was done considering only frames with the better quality flag ($ppErrBits < 16$) in all bands. For each ETG we selected the nearest UKIDSS detected galaxy within a matching radius³ of $1''$. 5080 ETGs have photometry available in all eight SDSS+UKIDSS filters.

² k-corrected with *kcorrectv4_1_4* (Blanton et al. 2003) through rest-frame filters blue-shifted by a factor $(1+z_0)$, adopting $z_0 = 0.1$ (see e.g. Hogg et al. 2004).

³ The matching was done with the *CrossID* form of the WFCAM Science Archive (see <http://surveys.roe.ac.uk/wsa/index.html> for details). Changing the matching radius to $0.5''$ leads to decrease the sample size by only five galaxies, confirming the accuracy of the matching procedure.

¹ We assume a Λ CDM cosmology with $\Omega_m = 0.3$, $\Omega_\Lambda = 0.7$, and $H_0 = 75 \text{ km s}^{-1} \text{ Mpc}^{-1}$.

TABLE 1
STATISTICS OF COLOR GRADIENTS.

$\nabla g - X$	μ	σ
g-r	-0.071 ± 0.003	0.121 ± 0.004
g-i	-0.084 ± 0.004	0.137 ± 0.003
g-z	-0.089 ± 0.006	0.173 ± 0.003
g-Y	-0.231 ± 0.006	0.171 ± 0.004
g-J	-0.279 ± 0.008	0.204 ± 0.005
g-H	-0.284 ± 0.008	0.194 ± 0.004
g-K	-0.297 ± 0.008	0.219 ± 0.005

3. COLOR GRADIENT ESTIMATES

The *grizYJHK* images of each galaxy were retrieved from the SDSS and UKIDSS archives, and processed with 2DPHOT (see La Barbera et al. 2008; hereafter LdC08). Galaxy images were fitted with PSF convolved Sersic models, allowing us to estimate structural parameters, i.e. the effective radius, r_e , the mean surface brightness within that radius, $\langle \mu \rangle_e$, and the Sersic index, n , homogeneously in all the bands. The PSF was accurately modeled⁴ in all wavebands by fitting the five closest stars to each galaxy with a sum of three Moffat functions, as detailed in LdC08. Having eight wavebands, seven different color gradients can be estimated. We used the parameters r_e , μ_e , and n , to estimate color indices, $g - X$ with $X = rizYJHK$, as a function of the distance, ρ , from the galaxy center. For each waveband, we estimate the mean surface brightness of the de-convolved Sersic model⁵ on a set of concentric ellipses⁶, whose ellipticity and position angle are fixed to the value of the *r*-band Sersic fitting. The color index $g - X$ at a given radius ρ is obtained by subtracting the mean surface brightness values at the corresponding ellipse. Each color profile is fitted in the radial range of $\rho_{min} = 0.1r_e$ to $\rho_{max} = r_e$ (see e.g. Peletier et al. 1990), by using an orthogonal least squares fitting procedure. We estimate the $g - X$ color gradients, ∇_{g-X} , as the logarithmic slopes of the $g - X$ profiles, $\nabla_{g-X} = d(g - X)/d(\log \rho)$.

4. CONSTRAINING AGE AND METALLICITY VARIATIONS

Considering the effect of age and metallicity, we write the equations:

$$\nabla_{g-X} = \frac{\partial(g-X)}{\partial \log t} \cdot \nabla_t + \frac{\partial(g-X)}{\partial \log Z} \cdot \nabla_Z, \quad (1)$$

where ∇_Z and ∇_t are the logarithmic radial gradients of age, t , and metallicity, Z , across the galaxy. The quantities $X_t = \partial(g - X)/\partial \log t$ and $X_Z = \partial(g - X)/\partial \log Z$ are the partial logarithmic derivatives of $g - X$ with respect to age and metallicity. The above linear equations hold if the color indices are continuous functions of t and Z , and the absolute values of ∇_Z and ∇_t are small.

From the operational viewpoint, we consider two stellar

⁴ For the PSF fitting in all wavebands, the mean value of the reduced χ^2 distribution amounts to ~ 1.04 , while the corresponding 90th percentile is 1.2.

⁵ Using the de-convolved models makes the procedure insensitive to seeing effects. We also verified that color gradients do not correlate with PSF fitting χ^2 values as well as with the error on the seeing FWHM, as estimated by 2DPHOT from the width of the *sure star locus* (see LdC08).

⁶ Ellipses are equally spaced in equivalent radius ρ by $0.01r_{e,r}$, where $r_{e,r}$ is the *r*-band r_e .

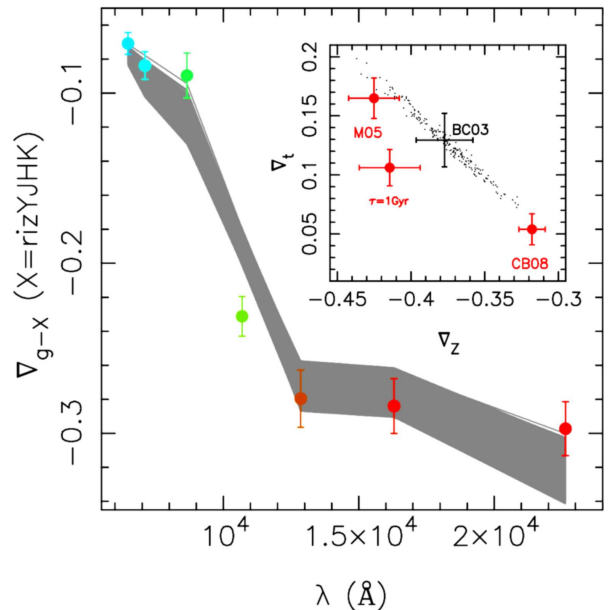


FIG. 1.— Mean color gradients, ∇_{g-X} (filled circles), as a function of the effective wavelength of the filter X . The error bars mark 2σ standard errors. The grey region shows the set of age and metallicity models that best match the observations (see text). The dots in the inset plots the best-fitted ∇_Z and ∇_t values obtained from the CB03 SSP models by shifting mean color gradients according to their uncertainties (see text). Variations in age and metallicity are generally correlated, making the dots to align along a narrow direction in the plot. The error bars are centered on the mean values of the best-fitted ∇_Z and ∇_t values, and mark the corresponding 1σ standard deviation. Different labels refer to the CB03 SSP model (black), and to the M05, CB08, and the $\tau = 1$ Gyr BC03 models (red).

populations and describe the properties of the galaxy at the inner and outer radii, ρ_{min} and ρ_{max} , respectively. Since our aim is that of characterizing stellar population gradients in the ETG population as a whole, we estimate the quantities ∇_Z and ∇_t from Eq. 1; using the mean values of the color gradient estimates⁷ ∇_{g-X} (see Sec. 5). We accomplish this in two steps: (i) We parametrize the colors available in terms of age and metallicity by using different spectrophotometric codes. We take simple stellar populations (SSPs) from Bruzual & Charlot (2003) (BC03), Maraston (2005) (M05), and Charlot and Bruzual (2008, in preparation; CB08). These SSPs are based on different synthesis techniques and have different IMFs. The M05 model uses the fuel consumption approach instead of the isochronal synthesis of BC03 and CB08. The CB08 code implements a new AGB phase treatment (Marigo and Girardi 2007). The IMFs are: Scalo (BC03), Chabrier (M05), and Salpeter (CB08). Moreover, we also use a composite stellar population model from BC03 having exponential star formation rate (SFR) with e-folding time of $\tau = 1$ Gyr⁸. The models are folded with the *grizYJHK* throughput curves, and flux

⁷ We verified that applying the same procedure to the single color gradient estimates, and then computing the mean values of ∇_Z and ∇_t changes these quantities by less than 0.02dex.

⁸ Though the determination of absolute values of age and metallicity at a given galaxy radius is beyond the scope of this paper, we have introduced the model with $\tau = 1$ Gyr since it is able to match also the absolute values of central colors in ETGs (La Barbera et al. 2003).

values computed for different values of t and Z . Here, we use ages spanning from 7.8 to 12.6 Gyrs⁹, and metallicities from 0.2 to $2.5Z_{\odot}$ for BC03 and CB08 models, and from 0.05 to $2Z_{\odot}$ for M05. To calculate the color derivatives with respect to t and Z , for each waveband we fitted the corresponding flux values with a two-dimensional eight order polynomial in $\log t$ and $\log Z$. The rms of the fits is smaller than 0.01mag for all the bands and models. (ii) We solve Eq. 1 in a χ^2 sense, by minimizing the expression

$$\chi^2 = \sum_X (\nabla_{g-X} - X_t \nabla_t - X_Z \nabla_Z)^2. \quad (2)$$

with respect to ∇_t and ∇_Z . We evaluate the derivatives X_t and X_Z at a given t and Z values, representing the average age and metallicity of the two stellar populations.

5. RESULTS

Table 1 lists the statistics of $g - X$ color gradients. We compute the peak value, μ , and the width, σ , using the bi-weight location estimator (Beers et al. 1990) taking 1000 bootstrap iterations to estimate uncertainties. As we can see, the peak value shifts to more negative values as we move to longer wavelengths, with a minimum $\mu \sim -0.3$ in $g - K$, and the width becomes progressively larger from the r to the K band. Because we have many galaxies, the random errors on μ and σ are very small.

Fig. 1 shows the mean color gradient, ∇_{g-X} , as a function of the effective wavelength of the filter X , where the trend reflects how stellar population properties vary, on average, as a function of radius in ETGs. We adopt the procedure described in Sec. 4 to infer the mean age (∇_t) and metallicity (∇_Z) radial gradients. To this end, we minimize Eq. 2 for each of the stellar population models described in Sec. 4. We estimate the quantities X_t and X_Z in Eq. 2 for $t = 10$ Gyr¹⁰ and $Z = Z_{\odot}$. Then, inserting the best-fit values of ∇_t and ∇_Z into Eq. 1, we derived the color gradient values that best-fit the observations. We performed $N = 1000$ iterations, shifting, each time, the observed mean color gradients according to the corresponding uncertainties. Each set of best-fitted color gradients defines a polygonal line in Fig. 1, obtained by connecting the best-fitting values of ∇_{g-X} . The grey region in the figure shows the area occupied by the $N = 1000$ bootstrap solutions. The inset shows the values of ∇_t and ∇_Z obtained from the different iterations. Computing the average and the standard deviation of these values, we obtain $\nabla_t = 0.13 \pm 0.02$ and $\nabla_Z = -0.38 \pm 0.02$, respectively. Using a different radial range for computing color gradients, with $\rho_{min} = 0.05r_e$ to $\rho_{max} = 2r_e$, does not change at all the values of the metallicity and age gradients. We also estimated ∇_t and ∇_Z by computing X_t and X_Z for different values of t and Z , varying t between 9 and 12 Gyrs, and Z between $3/4$ and $2Z_{\odot}$. The inferred absolute value of ∇_Z ranges from ~ 0.3 to ~ 0.4 dex, while the value of ∇_t is always positive, varying between ~ 0.01 and ~ 0.25 dex¹¹.

⁹ corresponding to a formation redshift of $z \sim 1.2$ and to the age of the Universe in the adopted cosmology

¹⁰ In the adopted cosmology; this age value corresponds to $z \sim 2.3$

¹¹ We obtain the minimum value of 0.01 only for the CB08 model, and only for the lowest metallicity case. For the BC03

6. DISCUSSION

We studied mean color gradients in ETGs using an unprecedentedly large and homogeneous sample with data from optical to NIR wavebands. We find that, on average, the main driver of color gradients is a radial variation of metallicity, and that a small, positive, age gradient seems to be present, on average, in ETGs, implying a mildly younger stellar population to the galaxy center. The mean metallicity gradient varies between $\nabla_Z = -0.32 \pm 0.02$ and $\nabla_Z = -0.425 \pm 0.02$, depending on the stellar-population model adopted to fit the color gradients. Previous studies based on much smaller samples, found ∇_Z mostly between -0.2 and -0.3 , with a typical uncertainty of ~ 0.1 (e.g. Peletier et al. 1990; Saglia et al. 2000; Idiart et al. 2002; La Barbera et al. 2003; Tamura and Ohta 2003; de Propris et al. 2004; Wu et al. 2005), consistent with what we find here.

Past literature has shown that age gradients do not explain color gradients, although a small positive age gradient of $\nabla_t \sim 0.1$ is still consistent with observations (see e.g. Saglia et al. 2000; La Barbera et al. 2003). For instance, Tamura and Ohta (2004) find a value of $\nabla_t = 0.1 \pm 0.14$, while Wu et al. (2005), analyzing optical-NIR color gradients for 36 nearby ETGs, report $\nabla = 0.02 \pm 0.04$. Here, we are able to detect a small but significantly positive age gradient in ETGs. The presence of younger stars in the center of ETGs is expected in most hierarchical formation scenarios. During the merger of gas-rich systems, gas dissipates its kinetic energy, falling into the galaxy center and forming stars. The detection of a positive age gradient also adds new insight to the fact that ETGs have smaller effective radii at higher redshift when compared to $z \sim 0$ (e.g. Daddi et al. 2005; Trujillo et al. 2006; Longhetti et al. 2007; Cimatti et al. 2008; Rettura et al. 2009; van der Wel et al. 2008; van Dokkum et al. 2008; Buitrago et al. 2008; Saracco et al. 2009). Since the luminosity evolution of a stellar population is approximately independent of its metallicity, the internal metallicity gradient of ETGs is assumed not to modify the effective radius with redshift. However, a difference in the formation epoch of two stellar populations corresponds to larger and larger differences in luminosity as we approach the formation epochs. Our result implies that a younger stellar population in the galaxy center would brighten more rapidly with redshift than the outer stellar population, making the profile more concentrated at high z , and possibly inverting the observed colour gradients. To quantify these effects, we take an $r^{1/4}$ law in the same radial range of ρ_{min} to ρ_{max} where we derived the internal color gradients (Sec. 3). At the inner radius ρ_{min} , we assume a stellar population with metallicity Z_{min} and formation redshift z_f . Then, for a given radius, the profile is evolved with redshift according to the luminosity evolution of a SSP whose age and metallicity are computed from z_f , Z_{min} , ∇_Z and ∇_t . At a given redshift, z , the profile is fitted with an $r^{1/4}$ law, yielding an effective radius $R_{e,z}$. We used three models with different values of z_f , ∇_t , and ∇_Z . We fixed $Z_{min} = Z_{\odot}$, since varying it in the range of $1/2Z_{\odot}$ to $2Z_{\odot}$ makes

and M05 models, we find $\nabla_t \gtrsim 0.1$ dex regardless of the t and Z values.

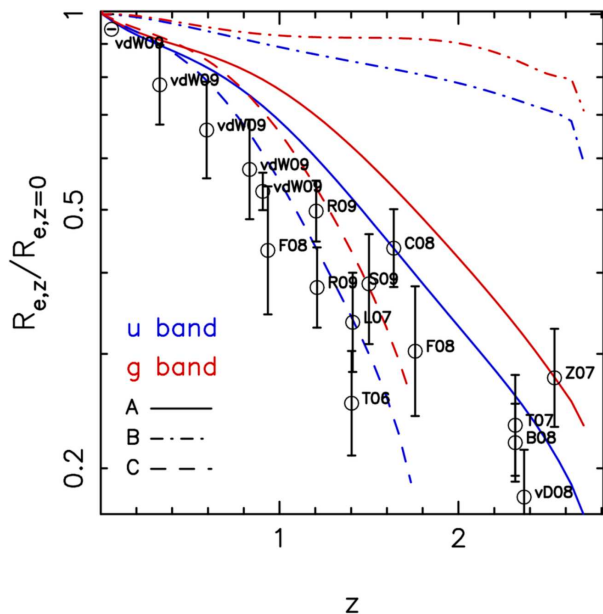


FIG. 2.— Evolution of the effective radius of ETGs as expected from different radial gradients of age and metallicity. Line types correspond to different age and metallicity gradient models, as shown in the lower-left of the figure (see the text). Circles with 1σ error bars show the observed evolution in size from previous studies (van der Wel et al. (2008), Saracco et al. (2009)).

$R_{e,z}$ change only a few percent. All the evolved profiles were well fit by the $r^{1/4}$ law, with an rms smaller than $\sim 0.05 \text{ mag/arcsec}^2$. Fig. 2 compares the evolution in size, $R_{e,z}/R_{e,z=0}$, from different sources in the literature with that expected from the three previously mentioned models. Since the data sample different rest-frames, from UV to optical wavebands, we constructed the models in both the u and g bands. Model A takes $z_f = 2.8$ and $\nabla_t = 0.08$, an age gradient consistent with our findings and such that the stellar population at ρ_{max} has an age limited by that of the Universe. Model B uses the same z_f as model A, but with $\nabla_t = 0$ and $\nabla_Z = -0.3$. Model C has the same metallicity and age gradients as Model A for BC03 SSPs, but a younger inner stellar population with $z_f = 1.8$. As expected, a pure metallicity model (Model B) does not predict any

significant size evolution with redshift. The evolution is mildly stronger in the restframe UV, with $R_{e,z}/R_{e,z=0}$ smaller in the u than in g band. At $z \sim 0$, the value of ∇_{u-g} is about -0.2 (Wu et al. 2005). Following the method of Sparks and Jørgensen (1993), this gradient implies that effective radii of ETGs increase by $\delta \sim 20\%$ from g to u band at $z \sim 0$. The waveband dependence of $R_{e,z}/R_{e,z=0}$ would tend to reduce and possibly invert this trend, producing $\nabla_{u-g} > 0$ at high redshift. The inversion takes place at a redshift, z_I , where the ratio of $R_{e,z}/R_{e,z=0}$ between the g and u bands equals the value of δ . For both models A and C, z_I is very close to z_f , being 1.6 and 2.4, respectively. Interestingly, positive color gradients in high-redshift ETGs have been detected by Ferreras et al. (2005), who found that about one-third of field ETGs at $z \sim 0.7$ have blue cores, in contrast to only 10% at lower redshift (see also Menanteau et al. 2001, 2004; Ferreras et al. 2009).

Fig. 2 shows that a single formation epoch for the inner stellar population of ETGs does not reproduce the observations. Model A predicts a size evolution of $\sim 80\%$ at $z \sim 2.4$, in good agreement with the data at $z > 2$. However, the evolution is too shallow for lower redshifts, where a smaller z_f is required to fit the data (model C). This result could be explained in a picture whereby ETGs form at different redshifts by gas-rich mergers, and the redshift-size trend is due to the increase in the amount of dissipation in mergers with redshift (Khochfar and Silk 2006). Fig. 2 suggests that the central bursts of star formation take place at different redshifts, above $z \sim 1.5$. However, the present analysis does not exclude a picture where the younger stars in the center form at very high redshift in most galaxies, with the color gradients accounting for only some part of the redshift-size relation.

We thank G. Djorgovski, I. Ferreras, R. Gal, and P. Saracco for several comments that helped to improve this paper. We thank the referee for helpful suggestions. We used data from the SDSS (<http://www.sdss.org/collaboration/credits.html>). This work is based on data obtained as part of the UKIRT Infrared Deep Sky Survey.

REFERENCES

- Beers, T.C., Flynn, K., & Gebhardt, K. 1990, *AJ*, 100, 32
 Bernardi, M., et al. 2003a, *AJ*, 125, 1849
 Blanton, M.R., et al., 2003, *AJ*, 125, 2276
 Bruzual, G., & Charlot, S. 2003, *MNRAS* 344, 1000 (BC03)
 Buitrago, F., et al. 2008, *ApJ* 687, 61 (B08)
 Cassata, P. et al. 2005, *MNRAS* 357, 903
 Cimatti, A., et al. 2008, *A&A*, 482, 21 (C08)
 Daddi, E. et al. 2005, *ApJ* 626, 680
 Faber, S.M. 1972, *BAAS* 4, 224
 Fan, L., 2008, *ApJ* 689, 101
 Ferreras, I., et al. 2005, *ApJ* 635, 243
 Ferreras, I., et al. 2009, *ApJ* 635, 243
 Franx, M., et al. 2008, *ApJ* 688, 770 (F08)
 Gómez, P.L., et al. 2003, *ApJ*, 584, 210
 Hogg, D.W., et al. 2004, *ApJ*, 601, 29
 Idiart, T.P., Michard, R., & de Freitas Pacheco, J.A. 2002, *A&A*, 383, 30
 Khochfar, S., & Silk, J. 2006, *ApJ* 648, 21
 La Barbera, F., et al. 2003, *A&A*, 409, 21
 La Barbera, F. et al. 2004, *A&A*, 425 797
 La Barbera, F., et al. 2008, *PASP*, 120, 681
 Lawrence, A., et al. 2007, *MNRAS*, 379, 1599
 Longhetti, M., et al. 2007, *MNRAS* 374, 614 (L07)
 Maraston, C. 2005, *MNRAS*, 362 799 (M05)
 Marigo, P., & Girardi, L. 2007, *A&A* 469, 239
 Menanteau, F., et al. 2001, *MNRAS*, 322, 1
 Menanteau, F., et al. 2004, *ApJ* 612, 202
 Peletier, R.F. et al. 1990, *A&A*, 233, 62
 de Propris, R., et al. 2004, *MNRAS* 357, 590
 Rettura, A., et al. 2009, *ApJ* in press (arXiv0806.4604) (R09)
 Saglia, R.P., et al. 2000, *A&A*, 360, 911
 Saracco, P., et al. 2009, *MNRAS*, 392, 718 (S09)
 Sorrentino, G., Antonuccio-Delogu, & V., Rifatto, A. 2006, *A&A*, 460, 673
 Sparks, W.B., & Jørgensen, I. 1993, *AJ* 105, 5
 Spolaor, M., et al. 2009, *ApJ* 691, 138
 Tamura, N., et al. 2000, *AJ* 119, 2134
 Tamura, N., Ohta, K., 2003, *AJ*, 126, 596
 Tamura, N., Ohta, K., 2004, *MNRAS* 355, 617
 Tinsley, B.M. 1973, *ApJ* 186, 35

Toft, S., et al. 2007, ApJ 671, 285 (T07)
Trujillo, I., et al. 2006, MNRAS 373, 36
Trujillo, I., et al. 2009, ApJL in press, arXiv:0901.1032
van der Wel, A., et al. 2008, ApJ 688, 48 (vW08)
van Dokkum, P., et al. 2008, ApJ 677, L5 (vD08)

Wu, H., et al. 2005, ApJ 622, 244
Zirm, A.W. et al. 2007, ApJ 656, 66 (Z07)